Molecular Systems Biology 6; Article number 391; doi:10.1038/msb.2010.52
Citation: ***Molecular Systems Biology*** **6:391**

www.molecularsystemsbiology.com

molecular systems biology

Kinase/phosphatase overexpression reveals pathways regulating hippocampal neuron morphology

William J Buchser, Tatiana I Slepak, Omar Gutierrez-Arenas, John L Bixby and Vance P Lemmon*

The Miami Project to Cure Paralysis, Departments of Pharmacology and Neurological Surgery, and Neuroscience Program, University of Miami, Miller School of Medicine, Miami, FL, USA
* Corresponding author. The Miami Project to Cure Paralysis, University of Miami Miller School of Medicine, 1095 NW 14th Ter., LPLC, Rm 4-16, Miami, FL 33136-1060, USA. Tel.: +1 305 243 6793; Fax: +1 305 243 3921; E-mail: vlemmon@miami.edu

Received 4.11.09; accepted 12.6.10

Development and regeneration of the nervous system requires the precise formation of axons and dendrites. Kinases and phosphatases are pervasive regulators of cellular function and have been implicated in controlling axodendritic development and regeneration. We undertook a gain-of-function analysis to determine the functions of kinases and phosphatases in the regulation of neuron morphology. Over 300 kinases and 124 esterases and phosphatases were studied by high-content analysis of rat hippocampal neurons. Proteins previously implicated in neurite growth, such as ERK1, GSK3, EphA8, FGFR, PI3K, PKC, p38, and PP1a, were confirmed to have effects in our functional assays. We also identified novel positive and negative neurite growth regulators. These include neuronal-developmentally regulated kinases such as the activin receptor, interferon regulatory factor 6 (IRF6) and neural leucine-rich repeat 1 (LRRN1). The protein kinase N2 (PKN2) and choline kinase α (CHKA) kinases, and the phosphatases PPEF2 and SMPD1, have little or no established functions in neuronal function, but were sufficient to promote neurite growth. In addition, pathway analysis revealed that members of signaling pathways involved in cancer progression and axis formation enhanced neurite outgrowth, whereas cytokine-related pathways significantly inhibited neurite formation.
Molecular Systems Biology **6**: 391; published online 27 July 2010; doi:10.1038/msb.2010.52
Subject Categories: functional genomics; neuroscience
Keywords: bioinformatics; development; functional genomics; metabolic and regulatory networks; neuroscience

Introduction

In neural development, neuronal precursors differentiate, migrate, extend long axons and dendrites, and finally establish connections with their targets. The initial steps of neurite formation and the subsequent specification of axons and dendrites have been widely studied. Clinical conditions such as spinal cord injury, traumatic brain injury, stroke, multiple sclerosis, Parkinson's disease, Huntington's disease, and Alzheimer's disease are often associated with a loss of axon and/or dendrite connectivity and treatment strategies would be enhanced by new therapies targeting cell intrinsic mechanisms of axon elongation and regeneration.

Phosphorylation controls most cellular processes, including the cell cycle (Vandenheuvel and Harlow, 1993), proliferation (Behrens *et al*, 1999), metabolism (Nimmo and Cohen, 1978), and apoptosis (Xia *et al*, 1995). Neuronal differentiation, including axon formation and elongation, is also regulated by a wide range of kinases and phosphatases (reviewed in Arimura and Kaibuchi, 2007). For example, the non-receptor tyrosine kinase Src (*Entrez symbol*: SRC) is required for cell adhesion molecule-dependent neurite outgrowth (Ignelzi *et al*, 1994) and the phosphatase Calcineurin (PPP3CA) is required downstream of calcium waves to transiently inhibit the extension of Xenopus spinal neurons (Lautermilch and Spitzer, 2000). In addition to individual kinases and phosphatases, signaling pathways like the MAPK, growth factor signaling, PIP3, cytoskeletal, and calcium-dependent pathways have been shown to impinge on or control neuronal process development (Lazarovici *et al*, 1987; Kuo *et al*, 1997; Morooka and Nishida, 1998; Wu and Cline, 1998; Huang and Reichardt, 2003; Menager *et al*, 2004; Chen *et al*, 2006).

Recent results have implicated GSK3 (Dill *et al*, 2008) and PTEN (Park *et al*, 2008) as therapeutically relevant targets in axonal regeneration after injury. However, these and other experiments have studied only a small fraction of the total kinases and phosphatases in the genome. Because of recent advances in genomic knowledge, large-scale cDNA production,

and high-throughput phenotypic analysis, it is now possible to take a more comprehensive approach to understanding the functions of kinases and phosphatases in neurons.

We performed a large, unbiased set of experiments to answer the question 'what effect does the overexpression of genes encoding kinases, phosphatases, and related proteins have on neuronal morphology?' We used a 'high-content analysis' approach to obtain detailed results about the specific phenotypes of neurons. We chose to study embryonic rat hippocampal neurons because of their stereotypical development *in vitro* (Dotti *et al*, 1988) and their widespread use in studies of neuronal differentiation and signaling. We transfected over 700 clones encoding kinases and phosphatases into hippocampal neurons and analyzed the resulting changes in neuronal morphology.

Many known genes, including PP1a, ERK1, p38, ErbB2, atypical PKC, Calcineurin, CaMK2, FES, IGF1R, FGFR, GSK3, PDK1, PIK3, and EphA8, were observed to have significant effects on neurite outgrowth in our system, consistent with earlier findings in the literature. Importantly, we also identified a number of genes not previously known to affect process growth. Combining the morphological data with information about protein sequence and molecular pathways allowed us to connect families of related proteins with novel functions in neurite development, and to implicate some signaling pathways in the regulation of neurite growth for the first time. Overall, our results provide a more complete picture of the kinases and phosphatases regulating neuronal growth, and suggest a number of testable hypotheses regarding the signaling pathways involved.

Results

A large-scale gain-of-function analysis in primary mammalian neurons

Electroporation-mediated transfection was used to overexpress kinases and phosphatases in embryonic rat hippocampal neurons. These neurons quickly adhere to laminin-coated plates, initiating neurite growth within hours (Esch *et al*, 1999). By 48 h, neurons typically possess several minor neurites and one major neurite (likely to develop into the axon) (Dotti *et al*, 1988). We marked transfected neurons by cotransfection with mCherry, a red fluorescent protein (RFP) (Shaner *et al*, 2004); transfection efficiency averaged 17.3% (95% confidence interval (95 CI), 16.6–18%) of the βIII-tubulin-positive neurons. Only transfected neurons were analyzed; neurons were defined as transfected (RFP+; Figure 1B and D, arrowheads) if their RFP intensities were greater than 2 s.d. above the mean of non-transfected controls (Figure 1E and F). Control experiments demonstrated that >80% of RFP+ neurons were cotransfected with the gene of interest (data not shown). Except when measuring the percent of neurons with neurites (%Neurite+), we considered neurons for further analysis only if they had at least one neurite >10 μm (Neurite+; Figure 1A and B) to avoid measuring potentially non-viable neurons (Figure 1C and D).

We obtained quantitative data for many cellular and neuronal morphological parameters from each neuron imaged. These included nuclear morphology (nuclear area and Hoechst dye intensity), soma morphology (tubulin intensity, area, and shape), and numerous parameters of neurite morphology (e.g. tubulin intensity along the neurites, number of primary neurites, neurite length, number of branches, distance from the cell body to the branches, number of crossing points, width and area of the neurites, and longest neurite; Supplementary Figure 1). Other parameters were reported on a 'per well' basis, including the percentage of transfected neurons in a condition (%RFP+), as well as the percentage of neurons initiating neurite growth (%Neurite+). Data for each treatment were normalized to the control (pSport CAT) within the same experiment, then aggregated across replicate experiments.

Validation of normalization and use of transfected neurons

We constructed a linear model incorporating experimental and treatment terms to test the validity of our normalization and our method for selecting transfected neurons (Figure 2C). The main sources of variance were the treatment (overexpression of kinases and phosphatases) and various aspects of experimental technique (animals, cells, time of prep, transfection, etc).

$$\mathrm{NTL}_{ij} = C + E_i + T_j + ET_{ij} + \varepsilon_{ij}$$

where C=constant, E=experiment effects, T=treatment effects, and ε=error.

The linear models fit the data appropriately, with coefficients of RFP− 0.62, 0.59 and RFP+ 0.87, 0.84 (for raw and normalized data models, respectively). The models were analyzed to determine the respective contributions of the treatment term (representing changes specifically because of overexpression), and the experimental term (representing noise). When analyzing cells defined as non-transfected, the experimental (noise) contribution predominated, both for raw and normalized data (Figure 2C). However, for cells defined as transfected (RFP+), the treatment effect increased (to 34%) and the noise contribution decreased (to 32%), even for raw data. For normalized data from transfected cells, the treatment contribution increased to 51%, whereas the experimental contribution became negligible (6%). We concluded that it was appropriate to analyze the RFP+ neurons, and that normalization significantly reduced the noise in the screen, revealing the effect of cDNA overexpression. Notably, the interaction term maintained a sizable contribution in our model (not shown), suggesting that a non-linear model would be able to explain more of the variance than our simple linear one.

Neurite number is regulated separately from neurite elongation

Correlations among the 19 normalized parameters were analyzed for neurons transfected with all kinase and phosphatase clones (Figure 2A). Primarily, this approach was taken to simplify the number of variables. Five groups of parameters as well as four single parameters emerged from the correlation analysis. Parameter groups comprised clusters of red intensity measures, soma geometry measures, neurite crossing, branching and neurite area, and neurite length measures (defined in

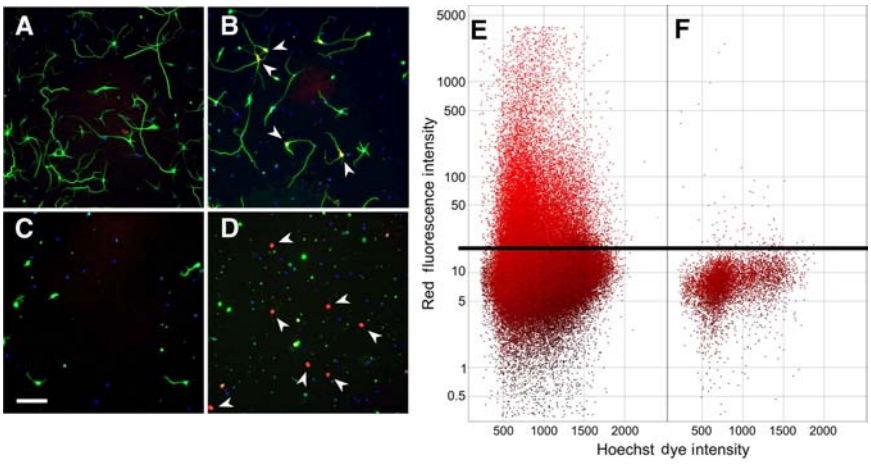

Figure 1 Hippocampal neurons assayed for neurite growth after transfection. (A–D) Hippocampal neurons growing on laminin, divided along two axes, producing four categories: Neurite + (**A**, **B**), neurons that have neurites, and Neurite− (**C**, **D**), neurons without. (A, C) RFP−, neurons that are not expressing red fluorescent protein (RFP) reporter. (B, D) RFP + neurons are expressing reporter, and thus are likely to be expressing the plasmid of interest. (B, D) RFP + neurons are identified by red cell bodies and arrowheads. (**E**, **F**) Scatter plots of RFP intensity from over 60 000 neurons in one experiment, plotted against nuclear (Hoechst) intensity. Each marker indicates one neuron. (E) RFP was added to the transfection as a reporter gene, and in (F) no reporter was added. Black horizontal line is transfection criterion. Scale bar=100 μm.

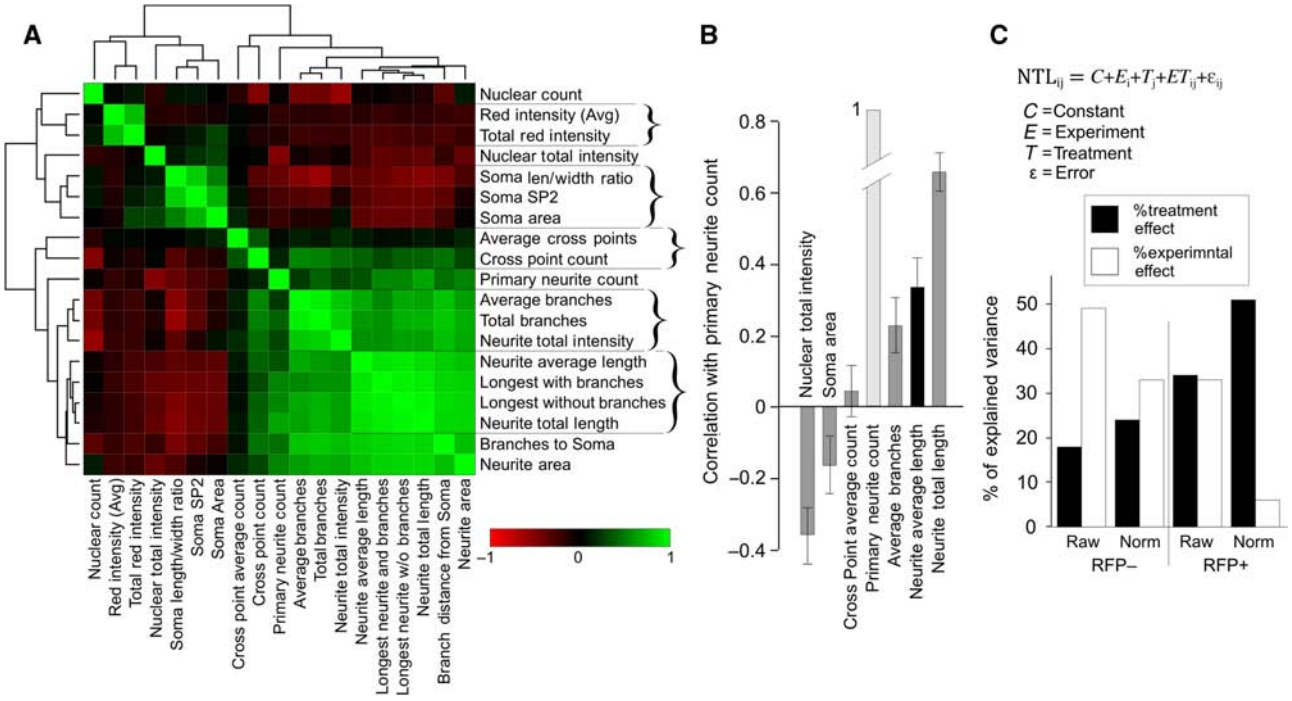

Figure 2 Morphological parameters reduced and normalization validated. (**A**) Clusters of correlated parameters were established by correlation between pairs. Braces indicate groups of closely related parameters. (**B**) Bar chart of correlation coefficients with primary neurite count. Bar chart depicts the correlation coefficient with 95% confidence intervals. (**C**) Generalized linear model developed to validate the population of cells to analyze. Top, Equation representing the explained variance from combinations of the experimental (E) effect and treatment (T) effect. Parameters were fit either as unnormalized raw values (Raw) or using relative change/normalized (Norm). We also considered the difference between untransfected (RFP−) and transfected (RFP +) neurons. By fitting the model to the equation NTLij for explained variance, very high fits were obtained for each group. The contribution from the treatment=signal (black bars) increased with transfected/normalized data, whereas the contribution from experimental variations=noise (white bars) decreased to 6% when using normalized, transfected data. Source data are available for this figure at http://www.nature.com/msb.

Supplementary Figure 1). On the basis of this analysis, the primary variables that define the neurite morphology are primary neurite count, neurite average length, and average branches. Interestingly, primary neurite count was not well correlated with neurite length or branching (Figure 2A). The Pearson correlation coefficient (r^2) between the number of primary neurites and the average length of the neurites was 0.332 (95 CI, 0.247–0.412), and between the number of primary neurites and average branching was 0.227 (95 CI, 0.146–0.302). In contrast, the correlation coefficient of average

branching with neurite average length was 0.670 (95 CI, 0.626–0.712) (Figure 2B). The primary neurite count was well correlated with neurite total length (NTL). This is expected as NTL is defined as (average length × primary neurite count) (Supplementary Figure 1).

There are at least two possible explanations for the low correspondence between primary neurite number and either neurite length or branch number. First, the number of primary neurites in embryonic hippocampal neurons could be very stable and imperturbable. Indeed, primary neurite number did not vary a great deal across the entire data set (2.13 ± 1.14 s.d.). However, we identified a group of genes (see below) that significantly perturbed primary neurite count, rendering this explanation unlikely. Therefore, a more likely possibility is that signaling mechanisms underlying the neurite number determination are different than those controlling length/branching of the neurites. A mechanism for this phenomenon has recently been examined (Shelly *et al*, 2010).

Phenotypic perturbation after overexpression of kinases and phosphatases

Neurons were transfected with each of 724 cDNA plasmids, from the NIH Mammalian Genome Collection (MGC) (Gerhard *et al*, 2004), mapping onto 622 different human and mouse genes. As 130 of these genes were orthologs, 492 unique genes were screened. After image/tracing validation, a number of clones were removed from the analysis (because of poor tracing or low cell number), leaving 449 unique genes (plus five control genes) in the final analysis.

To identify relevant functional classes of neuronal phenotypes, three key parameters were considered—primary neurite count, average length, and branching. Changes in these parameters resulting from gene overexpression were examined using hierarchical clustering (Figure 3). Of the 454 unique genes (including controls), 59 had statistically significant positive effects in neurite count and length, and are grouped on the left side of the heat map in green. Only nine genes increased both the primary neurite count and the average neurite length, whereas 23 genes increased neurite average length. An additional 32 genes increased the primary neurite count, but with little or no increase in length. Only a few of the genes assayed were significant determinants of both neurite length and neurite count. It is likely that these genes control general neurite initiation, whereas the other phenotypic classes regulate more specific cellular programs. A majority of genes with significant effects (92) were inhibitory to neurite growth.

We identified several genes that significantly altered neurite growth. For example, choline kinase α (CHKA) promoted positive growth enhancement for all parameters after over-

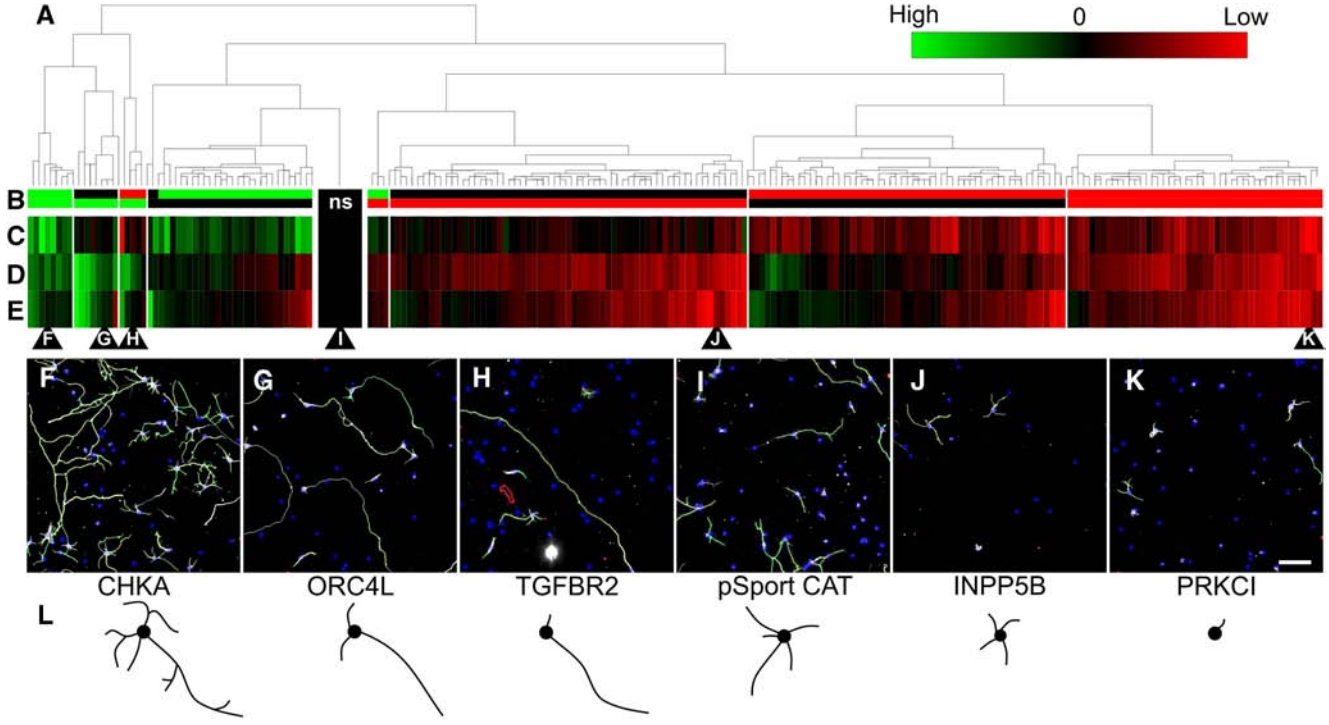

Figure 3 Phenotypic perturbation after kinase and phosphatase overexpression in hippocampal neurons. Overexpression of genes coding for particular kinases and phosphatases significantly perturbed neuronal morphology. (**A**) Dendrogram produced from hierarchical clustering sorted the genes by phenotype. (**B**) Blocks of color indicate significance and direction of effect for neurite count and neurite average length, where green indicates values significantly above control, red significantly below, and black not significant. (**C**–**E**) Heat map of genes that are significantly different from control, with three different parameters, neurite count (*C*), average length (*D*), and average branches (*E*), where green indicates a relative (normalized) increase, and red a decrease in value. Values for red and green are as follows, neurite count −0.25 to 0.3, neurite length −0.47 to 0.51, and branch points −0.51 to 1.66. Genes not significantly different than control were originally clustered above (**I**), indicated by 'ns.' (**F**–**K**) Six representative images of neurite growth with tubulin immunofluorescence (grayscale) and nuclear (blue), cell body (white), and neurite tracing (yellow/green) overlays. The Entrez Gene symbol is listed below the image (left to right: choline kinase, origin recognition complex like, TGF-β receptor, control (pSport-CAT), inositol polyphosphate-5-phosphatase, PKC iota). Black triangles indicate a gene's location in the cluster and heat map. (**L**) Cartoons of stereotyped neurite growth phenotype for each example image. Scale bar=100 μm. Source data are available for this figure at www.nature.com/msb.

expression in hippocampal neurons (Figure 3F). Origin recognition complex subunit 4-like and the TGF-β receptor 2, increased the length of hippocampal neuron processes (Figure 3G and H). Origin recognition complex was previously reported to regulate dendrite development (Huang *et al*, 2005). Inositol polyphosphate phosphatase (INPP5B) overexpression increased the number of primary neurites and led to decreased neurite length (Figure 3J). Although these genes had enhancing effects on laminin, they had little effect on neurite growth on the artificial substrate polylysine (Supplementary Figure 2). The strongest inhibitory genes produced very short neurites with only a few neurons initiating growth (e.g. atypical PKC iota, PRKCI; Figure 3K). These inhibitory genes did not generally affect survival (Supplementary Figure 3). Overall, we identified several neurite growth activators, and many neurite growth inhibitors in hippocampal neurons. The full table of results is provided in Supplementary Table 1.

Effects of known neurite-regulatory genes on neuronal morphology

We selected a group of genes that were tested in our experiments and had been previously implicated in neuron development, neuritogenesis, axon elongation, or neuronal polarity. Table I reports the results of overexpression of these genes in hippocampal neurons for four parameters: nuclear intensity (increases reflect nuclear condensation; Marcus *et al*, 1979), primary neurite count, neurite average length, and average branching. The latter three parameters were chosen because they defined the three distinct groups of neurite variables. Genes that had significant effects (after correction for multiple comparisons) are indicated. As expected, the protein kinase A catalytic subunit (PRKACA) and the atypical PKCs (PRKCI, PRKCH) strongly perturbed the neuron's phenotype. Overexpression of these kinases was sufficient to inhibit neurite growth. PKA activity has previously been suggested to affect growth on laminin negatively (Bixby, 1989), but also has been linked to positive regulation of neurite growth (Kao *et al*, 2002). It is possible that our (inhibitory) results with PKA reflect mislocalization because of expression of the catalytic subunit in the absence of the regulatory subunit. Note that although overexpression of PKA inhibited neurite length, it did not increase the nuclear intensity, suggesting cell death was not the cause (Table I). To determine whether PKA's effect was due to its kinase activity, we compared expression of wild-type PRKACA to that of an inactive mutant. Transfection of PRKACA led to strong inhibition of neurite growth (Figure 4B), whereas transfection of a kinase-dead mutant (K73A; Figure 4C) did not alter neuronal morphology (compare Figure 4A). Therefore, PRKACA's kinase activity was required for its inhibition of neurite growth.

Neuronal morphology is altered by expression of members of kinase and phosphatase families

Related proteins are often involved in similar neuronal functions. For example, families of receptor protein tyrosine phosphatases are involved in motor axon extension and guidance in both *Drosophila* and in vertebrates (Desai *et al*, 1997; Stepanek *et al*, 2005), and a large family of Eph receptor tyrosine kinases regulates guidance of retinotectal projections, motor axons, and axons in the corpus callosum (Brennan *et al*, 1997; Klein, 2001; Mendes *et al*, 2006). We therefore asked whether families of related genes produced similar phenotypes when overexpressed in hippocampal neurons. Our set of genes covered 40% of the known protein kinases (Supplementary Table 2), and many of the non-protein kinases and phosphatases.

Genes were sorted into one of five categories before the sequence alignment to produce distinct trees: protein kinases (Figure 5A), non-protein kinases (Figure 5B), protein phosphatases (Figure 5C), other phosphatases (Figure 5D), and other genes (Figure 5E). Phylogenetic trees were used to determine amino-acid similarity and infer evolutionary distance. Related families were thus clustered into branches and subbranches. Genes identified as protein kinases (Manning *et al*, 2002; Caenepeel *et al*, 2004) were aligned using the amino-acid sequences of the kinase domains only, whereas other genes were aligned by their entire sequences. The alignment successfully clustered the genes into known families. For example, the protein kinase tree (Figure 5A) matched the organization of previously identified protein kinase groups (Manning *et al*, 2002; Caenepeel *et al*, 2004). Also, 81% of the genes with obvious siblings (i.e. PPP2CA, PPP2CB) were linked to their sibling in the trees.

To establish the neuronal phenotype for individual genes within families, we plotted the functional data for NTL on markers overlying the trees (Figure 5). The neuronal response observed after the overexpression of individual kinases and phosphatases was diverse across gene families. Expression of most kinase and phosphatase genes reduced the length of the neurites compared with controls (Figure 5, red markers). Some families were particularly inhibitory. For example, BMP/activin receptors, PKAs/PKCs (PRKACx, PRKCx), and most protein serine/threonine phosphatases (PPP branch) inhibited neurite extension.

Gene families commonly exhibit redundant function (Urrutia *et al*, 1997; Xian and Zhou, 2004). Redundant gene function has often been identified when two or more knockouts are required to produce a phenotype (Heber *et al*, 2000). Our technique allowed us to measure whether different members of gene families had similar (potentially redundant) or distinct effects on neuronal phenotype.

To determine whether groups of related genes affect neuronal morphology in similar ways, we used sequence alignment information to construct gene clusters (Figure 6A). Genes were clustered at nine different thresholds of similarity (called 'tiers'). The functional effect for a particular parameter was then averaged within each cluster of a given tier, and non-parametric statistics were performed to determine the significance of the effect. Results from the neurite initiation parameter are shown in Figure 6B. Here, the giant cluster containing every gene has an average near control level and is colored white (Figure 6B, bottom tier, labeled 1 on the left). As the threshold is increased, clusters of fewer but more closely related genes are constructed, and their mean effect on the phenotype is displayed by the color of the rectangles in the heat map (red=decrease, green=increase, diamonds and asterisks indicate significance).

Table I Known neural growth regulators

1	2	3	4	Common name	Symbol	Note	Citations
				AKT2	AKT2	Inhibition correlated with decrease	Namikawa *et al* (2000)
				CAMK1d	CAMK1D	Inhibiting decreased length	Wayman *et al* (2004)
				CAMK1g	CAMK1G		
–	+++	++	+++	CAMK2a	CAMK2A	Slowed dendritic growth, mediates GABA induced neurite growth	Wu and Cline (1998); Borodinsky *et al* (2003)
–	––		–	CAMK2d	CAMK2D		
			+++	c-Src kinase	CSK	Inhibits neurite growth in PC12	Dey *et al* (2005)
				EGF receptor	EGFR	Activity-mediated inhibition	Koprivica *et al* (2005)
				ERK1	MAPK3	Activated form induces outgrowth	Kolkova *et al* (2000);
–	+			ERK2	MAPK1		Robinson *et al* (1998)
				EphA4	EPHA4	Better regeneration in EphA4 KO	Goldshmit *et al* (2004)
				EphA7	EPHA7	Better recovery after EphA7 reduction	Figueroa *et al* (2006)
++	––	–		EphA8	EPHA8	Induces MAPK activity to promote	Gu *et al* (2005)
–––			+++	ErbB2	ERBB2	Neuregulin promotes through erbB2	Bermingham-McDonogh *et al* (1996)
				FAK	PTK2	GF + Integrin > FAK > PC12 growth	Ivankovic-Dikic *et al* (2000)
+++	––			FES	FES	Accelerates NGF-induced PC12	Shibata *et al* (2003)
+++				FGF receptor1	FGFR1	Overexpression-promoted outgrowth	Hausott *et al* (2008); Lin *et al* (1996)
	–––			FGF receptor4	FGFR4		
				Fyn related (GTK)	FRK	Induces NGF-independent PC12 growth	Anneren *et al* (2000)
				FYN	FYN	Fyn-mice lack NCAM neurite growth	Beggs *et al* (1994)
		––	–	GSK3A	GSK3A	Has distinct function from below	Yoshimura *et al* (2005); Lee *et al* (2007)
				GSK3B	GSK3B	Inhibition of GSK3b promotes	Yoshimura *et al* (2005)
	––		–	IGF1 receptor	IGF1R	Receptor is essential for Hipp polarity	Sosa *et al* (2006)
				ILK	ILK	Overexpress Wt ILK stimulates growth	Ishii *et al* (2001)
				JNK2	MAPK9	JNK required for axon formation	Oliva *et al* (2006)
	+			JNK3	MAPK10		
				MARK2	MARK2	Ectopic express led to loss of axons	Chen *et al* (2006)
				MEK3	MAP2K3	MEK required for TrkB growth	Atwal *et al* (2000)
				MEK5	MAP2K5		
		++	++	ORC4L	ORC4L	Knockdown-reduced branching	Huang *et al* (2005)
				PAK4	PAK4	Membrane targeting increase growth	Daniels *et al* (1998)
		–	––	PDK1	PDPK1	Activated by PI3K	Alessi *et al* (1997)
				PIK3	PIK3R1	PI3K inhibitors reduce axon elongation	Menager *et al* (2004); Da Silva *et al* (2005)
	–––	–	–––	PKA catalytic A	PRKACA	Inhibit PKA stops forskolin growth	Kao *et al* (2002); Chijiwa *et al* (1990)
+++				PKA catalytic B	PRKACB		
++	–	–		PKC eta	PRKCH	Cell polarity and Par complex	Chen *et al* (2006); Lin *et al* (2000)
+	––	––		PKC iota	PRKCI		
++				RAF1	RAF1	Activated raf–axon elongation	Markus *et al* (2002)
				SAD kinase	BRSK1	Required for polarization	Kishi *et al* (2005)
++				SRC	SRC	SRC KO impairs growth	Ignelzi *et al* (1994)
				p35	CDK5R1	Inhibits PAK	Nikolic *et al* (1998)
+	––			p38 a	MAPK14	Required for PC12 outgrowth; inhibiting enhances growth	Morooka and Nishida (1998); Myers *et al* (2003)
	–	–	–	p38 b	MAPK11		
				p38 d	MAPK13		
				p38 g	MAPK12		
		–	––	Calcineurin	PPP3CA	Ca ++ waves inhibit through Calcn	Lautermilch and Spitzer (2000)
	––	+	+++	PP1a	PPP1CA	Dephosphorylates PKA	Tang *et al* (2003)
+++				PTEN	PTEN	PTEN KO retinal regrowth after crush	Park *et al* (2008)
				PTPRa	PTPRA	Drosophila	Desai *et al* (1997)
				SHP2	PTPN11	NGF growth inhibited by mutant Shp2	Chen *et al* (2002)

In all, 48 kinases and phosphatases previously reported for their involvement in neural process development and polarity. Columns of the table refer to intensity of the Hoechst nuclear dye (1), primary neurite count (2), neurite average length (3), and average branching (4). Effect for each parameter (+ ,– $P<0.1$, ++ ,–– $P<0.05$, +++ ,––– $P<0.01$, corrected by Benjamini–Hochberg), compared with controls. Genes are identified by their common name, official Entrez symbol, and official full name. Genes are arranged with the kinases on the top, and the phosphatases below.

We analyzed results for this cluster analysis with the three key neurite parameters (average neurite length, primary neurite count, and average branching) in addition to the frequency of neurite initiation (from the percent of neurons with axons or dendrites). Genes that perturbed each of these phenotypes are grouped in Figure 6C. Eight families, most with only a few genes, produced significant changes for one or two parameters. A diverse family of non-protein kinases had a positive effect on neurite outgrowth in three of the four parameters analyzed. This family of kinases consisted of a variety of enzymes, mostly sugar and lipid kinases, with the strongest effects coming from IRF6 and CHKA.

Molecular pathways revealed by neuronal phenotypes

Over the past 10–20 years, literally hundreds of neuronal growth and regeneration-associated genes have been identified (e.g. Table I). However, determining which of these genes

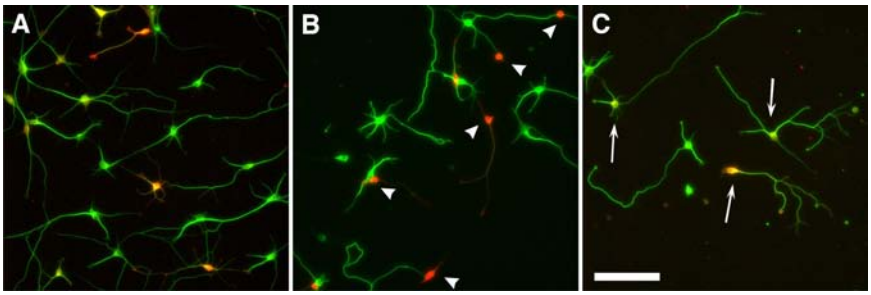

Figure 4 Overexpression of PKA catalytic subunit α inhibits neurite growth. Its kinase activity is responsible for the phenotype change. (**A**–**C**) Hippocampal neurons transfected with control (mCherry, A), PKA catalytic subunit α (PRKACA, B), and kinase-dead mutant of PKA (PRKACA K73A, C). Arrowheads indicate PRKACA-transfected neurons; arrows indicate neurons expressing the kinase-dead mutant of PKA. The neurons' processes are visualized by βIII-tubulin (green), and mCherry coexpression (red). Scale bar=100 μm.

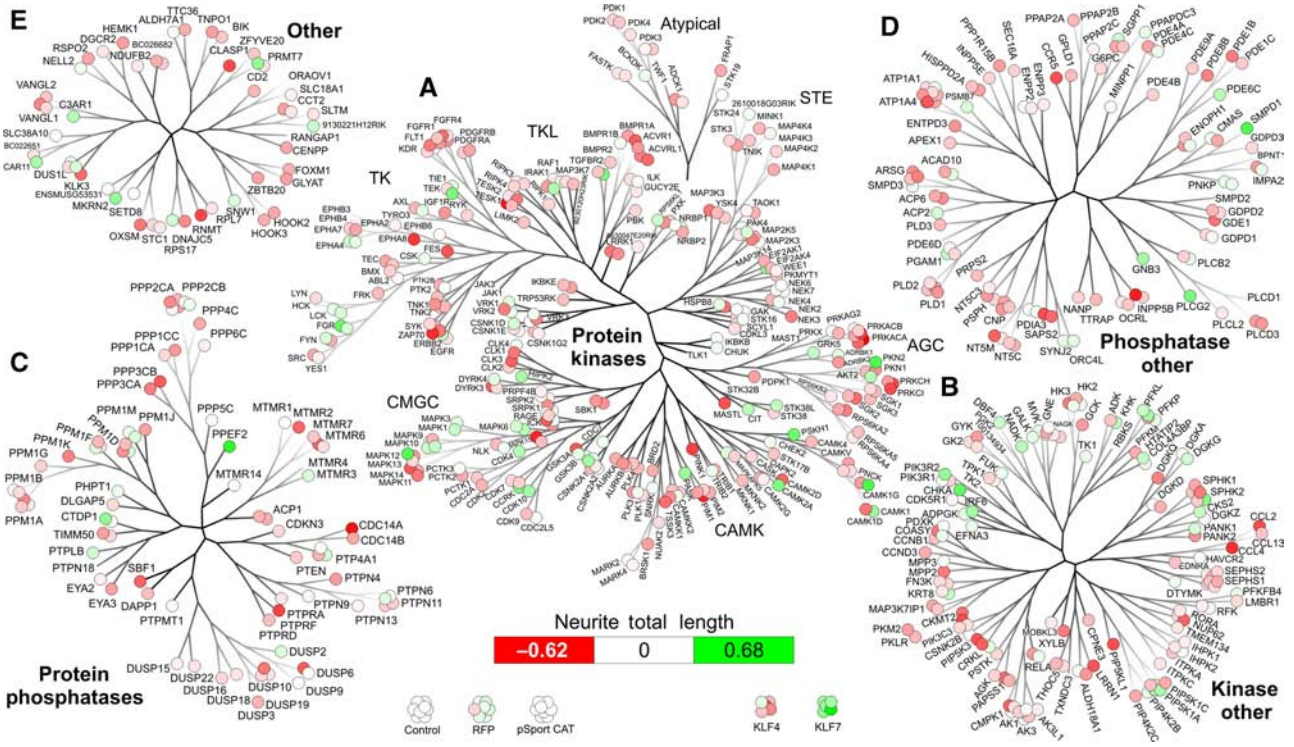

Figure 5 Families of kinases and phosphatases modify neurite outgrowth. Screened genes were aligned by sequence then displayed as phylogenetic trees, representing evolutionarily related proteins. Genes were separated into five primary categories, protein kinases (**A**), non-protein kinases (**B**), protein phosphatases (**C**), non-protein phosphatases (**D**), and others (**E**). Protein kinases were further subdivided into seven families (based on kinase domain sequences). Branch lengths on the trees represent the amino-acid change from parent to sibling and therefore the evolutionary 'distance' between genes. Labels beside the branches are the official Entrez Gene symbol. Circular markers were overlaid atop the trees, with the color of the marker indicating either no change in neurite length from control (white), an increase (green) or decrease (red). KLF4 and KLF7 are transcription factors that are regulators of neurite growth (Moore *et al*, 2009; Blackmore *et al*, 2010), and were included in the screen as additional controls. Source data are available for this figure at www.nature.com/msb.

are primary regulators of process development has been challenging. It is possible to refine the understanding of these genes with existing pathway information. One hurdle is that most genes with pathway annotations are members of multiple pathways. Of the 550 genes we successfully screened, 46% had pathway annotations, and of those, 66% were members of more than one pathway. Of the latter, half were members of four or more pathways. We performed pathway analysis for 79 different pathways in 24 categories using Kyoto Encyclopedia of Genes and Genomes (KEGG) (Kanehisa *et al*, 2004) (http://www.genome.jp/kegg/pathway.html) (Figure 7A and B). This analysis was displayed in the form of a heat map (Figure 7C). KEGG provided the classification of main categories (Figure 7A), subcategories (Figure 7E), and the pathways (Figure 7B). Genes were then placed in these pathway 'bins.' The color of the bin indicates the strength and the direction of the effect observed (Figure 7C and D). Pathways involved in proliferation of specific cancers, dorso-ventral axis formation, cytokine signaling, and ErbB signaling each had genes that were significant in their ability to modify neuronal morpho-

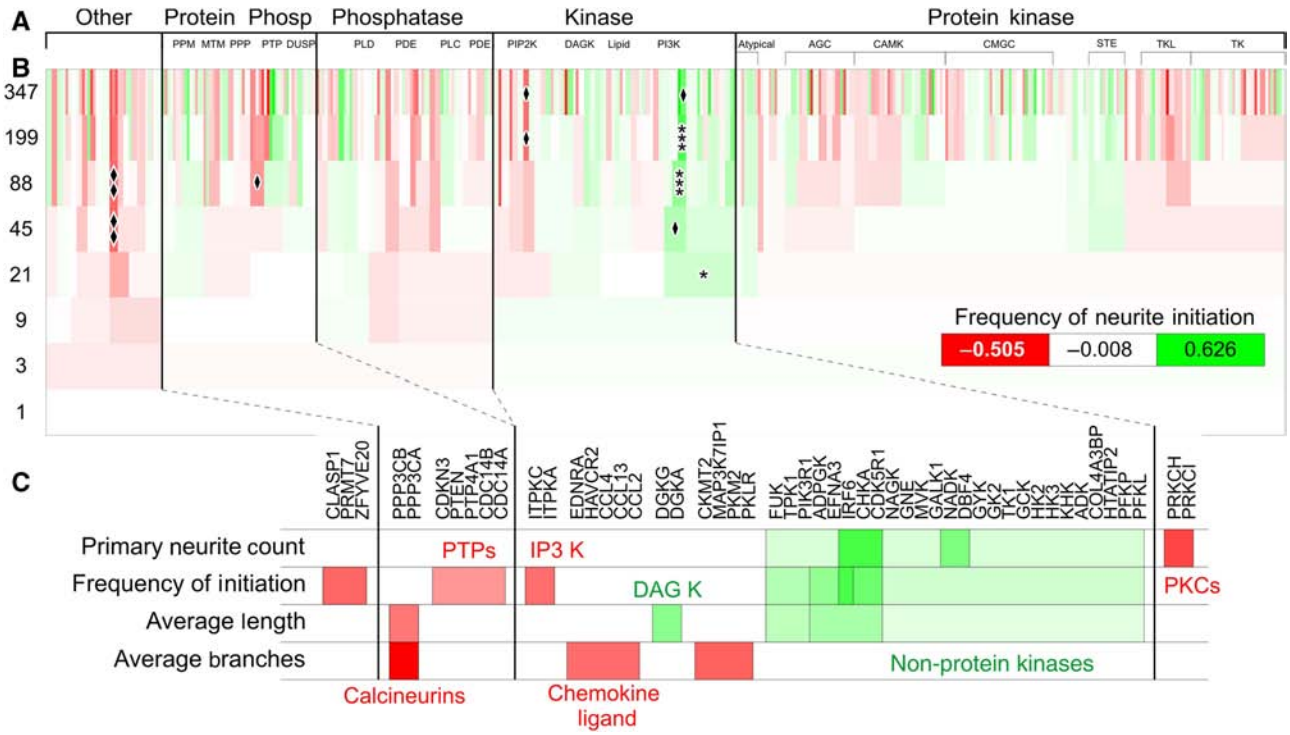

Figure 6 Bioinformatics identify putative families of active genes. (**A**) Genes overexpressed in hippocampal neurons, arranged by phylogenetic relationships (as in Figure 5, but 'unrolled') where the most closely related genes are next to each other. The five trees are preserved in the five sections (columns) of the graph. (**B**) Cluster heat map for the frequency of neurite initiation. At the bottom (labeled 1), all of the genes are combined into one large cluster, where there was no net effect on neurite growth (white). Going up from the bottom, genes are grouped in smaller, more focused families, with 3, 9, 21, 45, 88, 199, and 347 families per tier (row of the heat map). Each rectangle represents a family of genes (corresponding to the labels in A) that has a mean effect that reduced (red), or increased (green) neurite initiation. Non-parametric statistics were performed on each family, where diamonds indicate values for spiked bootstrap ($^P \leqslant 0.05$, $^^P \leqslant 0.01$). Asterisks indicate significance corrected by Benjamini–Hochberg ($^*P \leqslant 0.05$, $^{**}P \leqslant 0.01$, $^{***}P \leqslant 0.001$). (**C**) Compilation of significant families for four parameters: primary neurite count, frequency of neurite initiation, neurite average length, and average branching. Colored rectangles demarcate the extent of the family (for instance CDKN3, PTEN, PTP4A1, CDC14A&B), the color the direction and magnitude of the effect, with labels giving the common names for the genes. Note that the large family of non-protein kinases (from FUK to PFKL) has smaller nested families with even greater effects. The calcineurins (PPP3CA&B), and the kinases IRF6, CHKA, and CDK5R1, had the greatest ability to perturb neurite growth. Source data are available for this figure at www.nature.com/msb.

logy (Figure 7C). In addition, groups of pathways (as determined by KEGG pathways) such as the cancer pathways and amino-acid metabolism pathways had significant effects (Figure 7D). Summary data for the most significant results are shown for neurite length, branching, red intensity (from RFP cotransfection, does not equate with the level of expression of cotransfected gene), and soma area. The pathways most involved in producing the observed phenotypes included cancer, apoptosis, axis formation, adherens junctions, neuroactive ligand–receptor interactions, and ErbB signaling (Figure 7G). Complete results of pathway analysis are shown in Supplementary Figure 4. Pathway cluster analysis showed that individual genes that were members of groups (from known pathways) had similar activities when overexpressed in hippocampal neurons. In particular, pathways involved in cancer cell proliferation potentiated neurite extension and branching. Manipulations of genes in these pathways may be important to enhance axon or dendrite growth after injury.

Discussion

In a large-scale screen using high-content analysis of primary mammalian neurons, overexpression of distinct classes of kinases and phosphatases significantly perturbed neurite growth, primary neurite count, and branching. In all, 59 genes increased process development, whereas almost 20 genes were inhibitory. Of the inhibitory genes, the catalytic subunit of PKA was of particular interest because of its very strong effect on inhibiting neurite growth, and we demonstrated its kinase activity to be necessary for its effect. We tested 48 genes previously documented to be active in neurite growth, inhibition, and polarity. Of these, PP1a, ERK1, p38a, ErbB2, PKC eta and iota, calcineurin, CaMK2, FES, IGF1R, FGFR, GSK3a, PDK1, PIK3, and EphA8 had the strongest effects.

Our functional data provide substantial information about how groups of genes/proteins might relate. Through novel analyses, we determined that several families of evolutionarily conserved proteins had similar effects on neurite growth. In particular, calcineurins, CDC14s, IP3Kinases, cytokines, diacylglycerol kinases, a host of sugar and lipid kinases, and the atypical PKCs had similar effects across family members, suggesting the possibility of redundant function. If these proteins were individually targeted for loss-of-function experiments, it would be unlikely that single deletions would lead to a phenotype. Some of these gene families (the non-protein kinases, for example) have no known functions in neurite development, and represent novel targets for the control of neurite formation and extension.

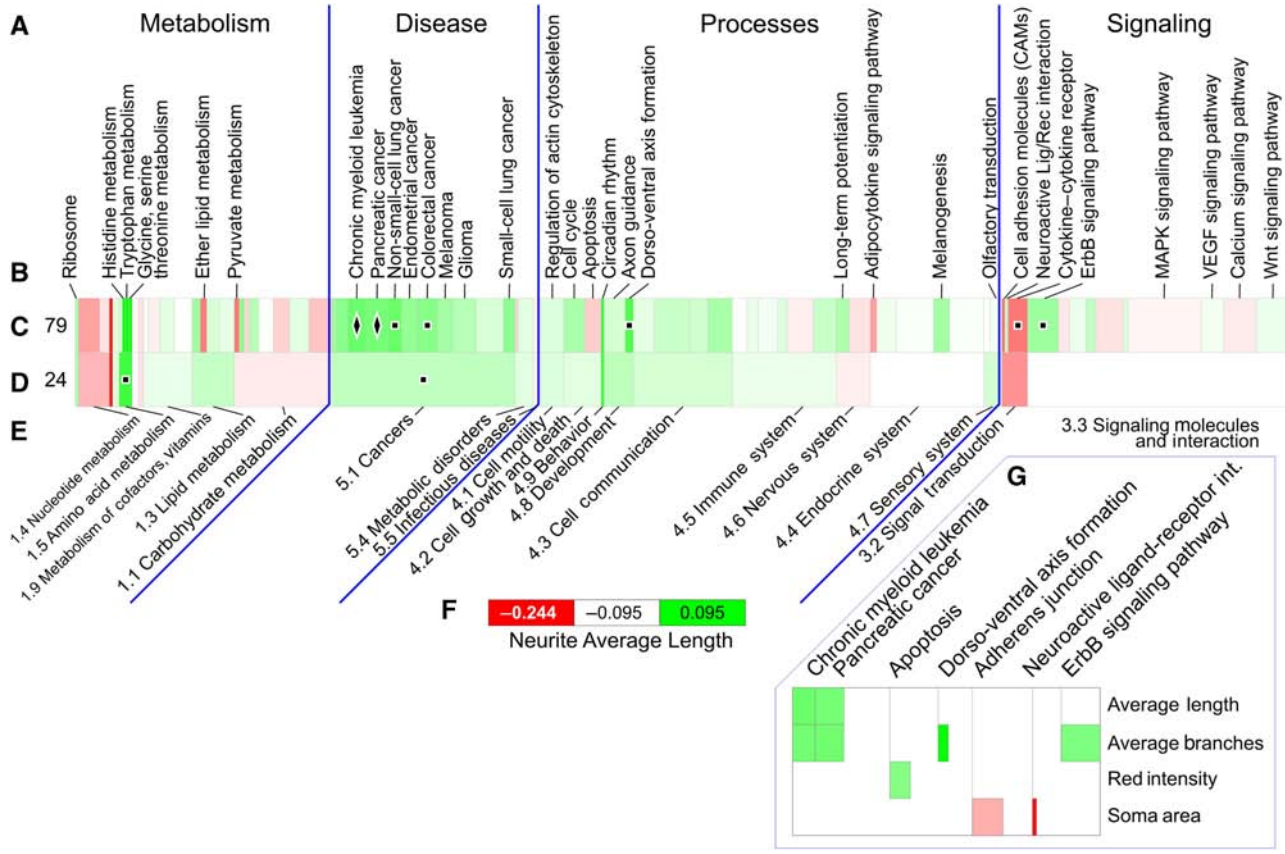

Figure 7 Neural process development is affected by known pathways, including cancer pathways. Pathway annotations from the KEGG grouped genes into 79 pathways. (**A**) KEGG categories. (**B**) KEGG pathway names. (**C**) Heat map for pathway's effect on neurite average length as indicated by color (red, decrease; white, no change from control; green, increase). (**D**) The 24 pathway subcategories, with heat map representing average effects of all genes in the category. (**E**) Names of pathway subcategories. (**F**) Legend for heat map. Symbols atop the heat map indicated significance from non-parametric statistics, where diamond is $P \leqslant 0.05$ by spiked bootstrap, and square is $P \leqslant 0.05$ by bootstrap. (**G**) After the analysis was repeated for four of the other parameters, the most significant pathways were compiled. They included three cancer pathways, the closely related ErbB signaling pathway, and dorsal-ventral axis formation pathway. Source data are available for this figure at www.nature.com/msb.

Pathways provide a conceptual framework to understand molecular dynamics in cells. We analyzed hundreds of genes for functional relationships, and found that several pathways implicated in cancer progression and dorsal-ventral pattern formation contain kinases and phosphatases with substantial abilities to alter neurite morphology.

Novel growth-associated genes

Our study uncovered a number of genes, including developmentally active genes, not previously linked to the regulation of axon/dendrite growth. For example, activin receptor 1 (ACVR1) is involved in Xenopus axis formation (Hemmati-Brivanlou and Melton, 1992) and downregulated during peripheral nerve regeneration (Morita *et al*, 1996). Both ACVR1 and ACVRL1 (and their isoforms) reduced neurite growth in our assays. IRF6 is also developmentally regulated during early development (Hatada *et al*, 1997) and its expression potentiated neurite growth in hippocampal neurons. CHKA, which strongly increased hippocampal neurite growth and neurite initiation, is an essential gene (Wu *et al*, 2008) that has been observed in nerve endings (synaptosomes) (Spanner and Ansell, 1979). Elucidating the mechanism through which CHKA influences neurite growth will be a fruitful future direction of study. SBK1 (SH3-binding kinase 1) is a novel and mostly uncharacterized serine/threonine kinase that is highly expressed in the brain (Nara *et al*, 2001). Two mouse clones of this gene with different UTRs inhibited neurite growth in our assays. Another serine/threonine kinase, microtubule-associated serine/threonine kinase-like (MASTL), which inhibited neurite outgrowth, is known to interact with microtubules. A non-protein kinase, neural leucine-rich repeat 1 (LRRN1), is highly expressed in early somitic myoblasts (Haines *et al*, 2005) and inhibited neurite growth when overexpressed.

Neurite growth activators were very rare in the AGC arm of the protein kinase tree, with the exception of protein kinase N2 (PKN2), known to be activated by Rho GTP, and regulate cell cycle proteins such as Cdc25B (Schmidt *et al*, 2007). Another AGC kinase, ribosomal protein S6 kinase/mitogen and stress activated kinase/p90rsk (RPS6KA4) inhibited neurite growth. RPS6KA4 has been shown to be required for CREB and ATF phosphorylation in fibroblasts (Wiggin *et al*, 2002), as well as being involved in cAMP and insulin-related proliferation (Coulonval *et al*, 2000). It has previously been implicated in regulating CAM-mediated neurite growth (Wong *et al*, 1996).

Two protein phosphatases, both members of the myotubularin family, significantly decreased neurite growth. Myotubularin related 2 (MTMR2) is known to be involved in myelin neuropathies, but is currently thought to act in Schwann cells, not neurons (Bolis *et al*, 2005). SET-binding factor 1 (SBF1) a pseudo-protein phosphatase, has been seen to decrease proliferation after its forced expression in fibroblasts (Firestein and Cleary, 2001). We observed SBF1 to decrease neurite growth after overexpression in hippocampal neurons.

Other genes with strong effects have either less known about them, or no obvious connection to neural function or pathways. The serine threonine kinase protein serine kinase H1 is involved in Golgi maintenance (Brede *et al*, 2003) and its overexpression enhanced growth. CMPK1 (cytidine monophosphate UMP-CMP kinase 1) a kinase involved in pyrimidine synthesis, inhibited neurite growth when overexpressed. The protein phosphatase protein phosphatase 1K was inhibitory, whereas protein phosphatase EF hand calcium-binding domain 2 (PPEF2) and sphingomyelin phosphodiesterase 1 acid lysosomal (SMPD1) were strong growth promoters in our screen, but the underlying mechanisms are unclear.

Candidates for future study from genetic and pathway analyses

Our phylogenetic analysis identified several families, such as the chemokine ligands, protein tyrosine phosphatases, and a large group of non-protein kinases, with members that strongly perturbed neurite outgrowth. Several of these were expected, especially the Calcineurins, Cdc14s, PI3K (Da Silva *et al*, 2005), and atypical PKCs. Other families were not expected to affect neurite growth, but did. These include a group of sugar kinases, NADK, and others. Not every member of this family had the same effect, but these enzymes generally potentiated neurite growth over control (surprising considering the neurons were growing on laminin, which strongly promotes neurite growth in the control state (Baronvanevercooren *et al*, 1982)). These non-protein kinases will be interesting to study to determine their functions in neuronal process development.

Pathway analysis revealed that genes in several cancer pathways were highly active. This is not unexpected, as growth of neurons is tied to the same cascades that lead to proliferation of cancer cells (Nakagawara, 2001). These pathways dominate the analysis, either because many of their genes were selected for study, and have been previously studied, or that these signals (as activated by overexpression) are quite strong compared with other pathways. Finally, the signal transduction pathways 'neuroactive ligand–receptor interaction' and 'cytokine–cytokine receptor interaction' have members that produced strong effects in opposite directions (Supplementary Figure 4, purple blocks). The study of these complete pathways will be an important undertaking for future analysis.

Comparison with other screens

Recently, three groups have used RNAi to test the necessity of various genes on neurite development or cell migration, which is likely to involve overlapping mechanisms (Enomoto *et al*, 2001; Maness and Schachner, 2007). Loh *et al* (2008) used the SH-SY5Y cell line in an siRNA screen of 750 kinases, many of which were also assayed in our experiments. Over half of the 'hit' siRNAs targeted genes in the tyrosine kinase or tyrosine kinase-like families. The intersection of hit genes from Loh *et al*, and genes from our study is listed in Supplementary Table 3. ERBB2, RYK, PRKAB1 enhanced neurite growth after overexpression in our assays and reduced neurite length after knockdown in the Loh screen. Conversely, PRKCI, PKN1, PDPK1 NEK3, MASTL inhibited neurite growth after overexpression in our assays and enhanced axon growth after knockdown in the Loh screen. Overexpression/knockdown of other genes (CDK9, FES, STK38L) led to the same phenotype in both screens. An siRNA screen by Sepp *et al* (2008) used *Drosophila* primary neurons to study the disruption of neural phenotypes in a genome-wide screen. They found that siRNAs for over 100 genes significantly perturbed neuronal phenotypes, leading to reduced elongation, excessive branching, loss of fasciculation, or blebbing (Sepp *et al*, 2008). The orthologs of four of the active genes from Sepp *et al* were also screened in our experiments. Two of these, ZAP70 and HTATIP, were weakly, but not significantly, inhibitory to neurite growth. Our analyses saw stronger effects (shorter neurites and more condensed chromatin) with the overexpression of LIMK2 and LRRN1 (see also Supplementary Table 3). Finally, Simpson *et al* (2008) performed an RNAi screen of kinase and phosphatases genes, assaying the ability of a monolayer of cells from a breast cancer cell line to heal after wounding. They found siRNAs targeting several genes that either potentiated or inhibited the migratory ability of the cells.

Comparing the results of these siRNA screens with each other, it is interesting to note that not a single gene appeared in all three. In fact, only three genes were hits in two of the three screens: BCAR3, LIMK1, and the JNK kinase MAP2K7. The lack of overlap in these RNAi screens supports the notion that such large-scale knockdown experiments require special analysis of the raw data for proper interpretation (Sacher *et al*, 2008). In our own unpublished experiments using siRNA and shRNA approaches, we have found it much more difficult to knock down protein expression in primary neurons than in cell lines. This is consistent with reports using transgenic mice expressing shRNAs; knock down in the CNS is less effective than in other tissues (Sasaguri *et al*, 2009). The slow and variable loss of protein expression using RNAi in neurons makes it a problematic strategy in a screening context. A recent high-content analysis of a genome-wide RNAi screen found that the majority of siRNAs have off-target effects (Collinet *et al*, 2010). Consequently, using RNAi in primary neurons as a screening approach will require much better validated libraries and assays that use novel approaches to allow protein expression to be knocked down before neurite growth starts (Davare *et al*, 2009). It is therefore critical to use alternative methods, such as overexpression.

Conclusion

Our studies have identified a large number of kinases and phosphatases, as well as structurally and functionally defined families of these proteins, that affect neuronal process formation in specific ways. We have provided an analytical

methodology and new tools to analyze functional data, and have implicated genes with novel functions in neuronal development. Our studies are an important step toward the goal of a molecular description of the intrinsic control of axodendritic growth. Downstream validation studies will be important to perturb the function of other members of the signaling cascades we have implicated, and to examine the functions of these genes in other neuronal types.

Materials and methods

Plasmid cDNA library

A glycerol stock cDNA library from the NIH MGC (Gerhard *et al*, 2004) in 96-well format was purchased from Open Biosystems (ThermoFisher, Huntsville, AL) that included IRAT (human) and IRAV (mouse) clones. The library was replicated and the original and daughter plates stored in −80 degree freezers, sealed with foil tape (Corning Costar 6570, Lowell, MA). The Gene Ontology (http://amigo.geneontology.org/) was consulted to determine an up-to-date list of kinases and phosphatases. Gene ontologies for 'Kinase Activity,' and 'Phosphoric Ester Hydrolase activity' were used to generate a list of kinases, phosphatases, and interacting genes. A custom program written on the Qiagen BioRobot-3000 (Germantown, MD) picked clones from the glycerol stock plates into the kinase-phosphatase sublibrary, which totaled nine 96-well plates. During the cherry-picking process, a set of 10–12 plates were thawed, wiped, uncapped, and the foil cover carefully removed. Disposable tips were used to inoculate media in deep-well 96-well blocks. During the process, glycerol stocks for mCherry (Shu *et al*, 2006) were also picked and inoculated into specified control wells on the plate. Other wells were left empty, to facilitate non-transfected controls and to allow other clones to be tested.

Plasmid preparation

QIAprep 96 Turbo BioRobot Kit (Qiagen 962141) was used to produce transfection quality plasmid. Briefly, two deep-well blocks from the kit were filled with 1.4 ml Terrific Broth (Invitrogen 22711, Carlsbad, CA) with 150 μg/ml ampicillin (Invitrogen 11593) in each well. A 96-pin replicator tool (Nalge Nunc 250520, Rochester, NY) was used to inoculate the thawed glycerol stock plate into fresh media. Plates were incubated for 20–24 h at 37°C, shaking at 300 r.p.m. The plates were spun down serially such that the pellets were overlaid and concentrated. The pellets were resuspended in Qiagen's 'P1' buffer, and the manufacturer's instructions were followed. Elution was performed at room temperature, with 120 μl of endotoxin-free water.

Plasmid concentration was analyzed with NanoDrop spectrophotometer (Thermo Fisher, Wilmington, DE). Plasmid was generally purified at 300 ± 100 ng/μl with an average 260/280 ratio of 2.8. If plasmid concentrations were below 300, plasmids were concentrated by isopropanol precipitation.

Kinase-dead PRKACA mutant

The kinase-dead mutant of human PRKACA was obtained by substituting lysine at position 73 for alanine (G→A substitution in AAG triplet coding for lysine). This was achieved by PCR using the QuickChangeII site-directed Mutagenesis Kit (Strategene) with the following primers: K73A sense 5′-GGAACCACTATGCCATG**G**AGATCCT CGACAAACA-3′; K73A anti-sense 5′-TGTTTGTCGAGGATCT**C**CATGGCA TAGTGGTTCC-3′. The resulting construct was verified by restriction analysis using the newly created NcoI site (underlined in the sense primer) and sequencing.

Neuronal cell culture

Embryonic hippocampal culture has been described earlier (Goslin *et al*, 1998; Oliva *et al*, 2006). Briefly, adult pregnant Sprague-Daley rats were euthanized by CO_2 and the E18 embryos were dissected in fresh Hibernate media (BrainBits, HE-Ca 500, Springfield, IL) supplemented with B27 (Invitrogen 17504). Isolated hippocampi were transferred to Hibernate media without B27 and incubated for 15 min at 37°C with 0.25% Trypsin (Invitrogen 25300), in the presence of DNaseI at final concentration of 0.5 mg/ml (Sigma D5025). The tissue was then washed five times with the same medium supplemented with B27 and triturated until no clumps were visible (about 5–10 times). Dissociated neurons were counted and used for transfection during the next 2 h.

Transfected and non-transfected neurons were grown in 96-well plates (Perkin Elmer, 6005182, Waltham, MA) coated with 10 μg/ml Poly-D lysine (Sigma P7886), and 10 μg/ml laminin (Sigma L2020). When cells were plated on PLL (Sigma P2636) alone as a substrate, the concentration was 1 mg/ml. Enriched neurobasal medium (ENB), modified from Meyer-Franke *et al* (1995) included Neurobasal (Invitrogen 12348), penicillin/streptomycin, insulin (Sigma I6634 5 mg/ml), sodium pyruvate (1 mM), transferrin (Sigma T1147 100 mg/ml), BSA (Sigma A4161 100 mg/ml), progesterone (Sigma #P8783 60 ng/ml), putrescine (Sigma P7505 16 mg/ml), sodium selenite (Sigma S5261 40 ng/ml), triiodo-thyronine (Sigma T6397, 1 ×), L-glutamine (1 mM), *N*-acetyl cysteine (Sigma A8199NAC, 5 mg/ml), and B27. Media was also supplemented with CNTF (10 ng/ml).

Transfection

Transfection of embryonic hippocampal neurons was accomplished using the Amaxa 96-well 'Shuttle' nucleoporation system (Lonza, Walkserville, MD) following the manufacturer's instructions. Briefly, the Amaxa 96-well nucleoporation plate was loaded with the mixture of 75 000 neurons in 20 μl of Amaxa transfection solution, and 400 ng of total DNA (including mCherry reporter with ratio plasmid to reporter 6:1) in a volume of 2 μl. The rat neuron transfection, 'high-efficiency' program was used, and the neurons were recovered with 80 μl of ENB + HEPES (20 mM, Invitrogen 15630). Several control plasmids were used including pSport mCherry (reporter alone) and pSport CAT, a plasmid with no CMV promoter (chloramphenicol acetyltransferase gene). Cells were then plated at two different densities—8000 and 12 000 cells per well. Transfection efficiency was validated by cotransfecting mCherry with plasmids from the library containing myelin basic protein, vimentin, GFAP, and NCAM cDNAs and subsequent identification by antibody staining (data not shown).

Fix/stain

Neurons were incubated in 37°C 5% CO_2 incubators for 48 h. Plates were removed and immediately fixed with room temperature 4% PFA, 4% Sucrose in PBS by removing 50 μl of medium and underlaying 120 μl of fixative for 30 min. Plates were rinsed with PBS and stained with anti-βIII-tubulin (Aves Labs, TUJ) and Hoechst dye (Invitrogen 33342).

Imaging/tracing

Cellomics KineticScan Reader (Thermo Scientific Cellomics, Pittsburgh, PA) was used to automatically image nine fields in each well of the plates at × 10 magnification in three different channels for nuclear staining (Hoechst), neurite staining (βIII-tubulin), and the reporter gene (mCherry). Images were traced automatically using the Neuronal Profiling Bioapplication version 2.x. For most of the downstream analysis, only the Transfected+ and Neurite+ populations were analyzed. Reported neurite measures are listed in Supplementary Figure 1. Other parameters were not analyzed because of high variability in the controls. Supplementary tables include complete results. Images and other data sets are available on request.

Overview

Neurons were transfected and plated in six replicate wells for each cDNA plasmid, at two different densities. Two independent experi-

mental replicates were performed for each of the clones. The clones that changed the morphology of the neurites reproducibly were transfected a third time. Over 10 000 wells were imaged and analyzed, each with nine fields, and one field from each well was manually annotated to check the quality of the automated tracing. The annotation identified acute errors that led to the images being removed from the data set (mostly because of poor focus). The resulting data were normalized (see below) so that the resulting value indicated difference from control for each parameter.

Analysis

Data aggregation/storage

Raw data were managed by the Cellomics Store, which consists of an SQL database and a network-attached fileserver (HP). Raw data consisted of metadata associated with scanning and tracing (exposures, focus offsets, thresholds), raw images and the results of the tracing. In addition, cell and well level data were exported and stored on a separate fileserver, organized by experiment with accompanying Excel tables listing how particular wells were treated.

Spotfire DecisionSite (Tibco) was used to associate the treatment variables (which plasmids were transfected in which wells) and perform basic quality control, including checks for tracing errors, low-and high-density wells, cell clumps, and plating errors.

Tracing quality control

Tracing was validated several times by comparison with Neurolucida tracing (MicroBrightField, Williston, VT). For validation of the tracing in the screen, an image of the tubulin channel from the first field of every well in each plate (over 10 000 images) was exported as a jpeg. Then, three annotators ran a custom C# program on their desktop computers that displayed the image and gave several options as to the quality of the focus, threshold, tracing, and cell density. The combined data from the annotators were used to either retrace plates or eliminate wells from the analysis.

Transfection threshold

By examining the red fluorescent intensity of the neurons that were not transfected with plasmid, a background amount of intensity was established using Spotfire DecisionSite, and used as a threshold for the classification of neurons as transfected. Within each experiment, a transfection threshold was defined using the distribution of the average red intensity (AI) of each cell in control neurons that were not subjected to nucleofection. This distribution was near to log-normal. Treated cells with a log(AI) higher than mean $+2$ s.d. of the control log(AI) were considered transfected. Only transfected cells were included in the analysis.

Normalization

The morphometric data of transfected cells in each treatment were normalized with respect to a control within the same experiment. We have observed that experiments, defined as the sequence 'isolation of neurons/transfection/culture/staining/imaging,' are a major source of variation. The controls are neurons that were subjected to transfection with the transfection marker and the plasmid pSport CAT as well as the reporter mCherry. After normalization, the variables for a given treatment were aggregated across the N replicate experiments where the treatment was present. Briefly, two different normalizations were used.

The first, rx, expresses the difference between control and treatment relative to the control,

$$rx = \frac{\overline{x_c} - \overline{x_t}}{\overline{x_c}}$$

where $\bar{x}_t$ and $\bar{x}_c$ are the means of the treatment and the control for variable x.

This normalized variable is aggregated across the N experiments, according to,

$$rx_{\mathrm{agg}} = \frac{1}{2} \cdot \sum_{i=1}^{N} \left(\left(\frac{n_{ti}}{\sum_{i=1}^{N} n_{ti}} + \frac{n_{ci}}{\sum_{i=1}^{N} n_{ci}} \right) \cdot rx_i \right)$$

where n_{ti} and n_{ci} are the cell number of the treatment and the control in experiment i. This normalization is intended to express the biological effect of the treatments disregarding its statistical significance given that it is not dependent on sample size and dispersion.

To estimate the statistical significance of the effects produced by any treatment, a different normalization was used. It is a t-value that is aggregated as a simple sum across the N replicated experiments. The statistical significance of this sum is computed from the convolution of N Student distributions each with $n_{ti} + n_{ci} - 2$ degrees of freedom.

Linear model

A generalized linear model for the NTL as a function of experiment and treatment was built to evaluate the quality of cotransfection-based cell selection, the normalization scheme and the inter-experiment variability.

$$\mathrm{NTL}_{ij} = C + E_i + T_j + ET_{ij} + \varepsilon_{ij}$$

where C is the overall average NTL, E_i represents the effect of the ith experiment, T_j represents the effect of the jth treatment, and ET_{ij} represents the interaction between E_i and T_j. This model was fitted to the NTL data from four (j=1…4) controls, pSPORT CAT, RFP, KLF4, and KLF7 across eight experiments (i=1…8). KLF4 and KLF7 are genes that systematically affect neurite growth (Moore *et al*, 2009). The variable NTL was analyzed in its original form and after the two normalization procedures for both transfected and non-transfected cells analyzed independently. Thus, the model was fitted to six different data sets, each of them with 64 data points ($8 \times 4 \times 2$ seeding densities), producing 32 degrees of freedom for the error ε_{ij} that is assumed to be independent and identically distributed with mean=0.

Correlation analysis

A Pearson correlation was applied to normalized data. Bootstrap resampling was used to construct a CI for the correlations using custom software written in C# with Microsoft Visual Studio 2008. During bootstrapping, pairs of values were taken by replacement n times to reconstruct a bootstrap replicate of the entire population. That process was then repeated 10 000 times, and the correlation coefficient was stored for each run. CI is reported as the top and bottom 2.5% correlation coefficients.

Neuron survival

Nuclear size and intensity of DNA staining (Hoechst) have long been used as indicators of the live/dead status of cells. Small and bright nuclei are the result of heterochromatin condensation, a hallmark of apoptotic cells death. Big and dim nuclei correspond to cells that are alive. We use this distinction to measure the cell survival of our cultures transfected with a variety of cDNAs, placing emphasis on those cDNAs that we found to significantly reduce neurite outgrowth.

In most instances, the clusters of live and dead cells in the nuclear area versus intensity were easily distinguished. Semi-supervised classification was implemented using three categories (live, dead, out of range) using a custom script in MatLab and was run on data on a plate-by-plate basis. The survival rate varied as a function of the transfection and neurite-bearing status. The RFP+ cells with neurites (N+RFP+), showed the highest survival rate.

As a measure of whether survival rates in treatments reducing neurite growth were significantly lower, cells in which cDNA for RFP was transfected with 240 ng of DNA were used as controls (same amount of cDNA used in the screen). Z factors were computed within each experiment using the mean and the s.d. of the control. The results within each treatment per replicate experiments were averaged and significance was computed using a permutation test. Supplementary

Figure 3B shows the signed significance for the effect of genes on survival. The signed significance is the absolute value of the log10 (*P*-value) multiplied by the sign of the *Z* factor. A signed significance of $\leqslant -2$ means that survival of the treatment is significantly lower than the control.

Bioinformatics

Phenotype clustering

After averaging values from genes that were represented by two species or multiple clones, phenotypic classes were determined by taking a discrete measure of significance (−1 significantly below control, 0 not significant, and 1 significantly above control at $P \leqslant 0.05$) and clustering to form distinct groups based on neurite average length and primary neurite count. Clustering was performed on the average values for neurite average length, primary neurite count, and branching with the main groups 'stratified' by the prior discrete clustering. The hierarchical clustering algorithm used normalized phenotypic data as well as the statistical status of each gene, but did not consider which genes were transfected or to what classes they belonged. This led to the arrangement in Figure 3. Hierarchical clustering was performed in Spotfire DecisionSite using clustering algorithm UPGMA and Euclidian distance.

Phylogenetic trees

Genes were grouped into five main categories, based primarily on their gene ontology information, but additionally hand curated to ensure higher accuracy. Most protein kinases were considered only if they were listed in one of the kinome references (Manning *et al*, 2002; Caenepeel *et al*, 2004). A few genes had ambiguous classification as they interacted with both kinases and phosphatases or had reported activity but no obvious enzymatic domain, etc. The process of tree creation is outlined graphically in Supplementary Figure 5. Protein sequence was obtained from the gene's Entrez Gene (http://www.ncbi.nlm.nih.gov/sites/entrez?db=gene) entry, and loaded into EBI's ClustalW2 (http://www.ebi.ac.uk/Tools/clustalw2/) (Thompson *et al*, 1994; Larkin *et al*, 2007) for each group separately in FASTA format. The output of the cluster algorithm is a dendrogram file, which represents the hierarchy in a nested text format [i.e. (Parent(Child A:0.2,ChildB(GrandchildA:0.13,GrandchildB:0.1):0.3))]. The dendrogram file is read into custom software, which parses the dendrogram and represents it as a binary tree, which can be drawn automatically in CorelDraw (X3, Corel Corporation, Mountain View, CA) as a radial, centered tree. Branch lengths in the tree correspond to the log of the distance as reported by ClustalW2. The angles of the branches and the order of the two segments from a branch are arbitrary and cosmetic. Some branches have multiple markers, indicating different clones that were tested for that gene (human and mouse as well as clone variants of the same species). Other branches have no marker, indicating one of the following; the gene was screened but the replicates failed, there were too few cells to analyze (possibly a viability defect), or failed tracing or image validation.

Phylogenetic gene cluster analysis

Phylogenetic relationships (from above) were transformed into a table where the columns represented nodes of the tree (except the leaves), and records were the genes. Values were binary representations of a gene's presence in that node (the column representing the node would get a 1 for presence or 0 for absence). That table was imported into Spotfire and hierarchical clustering (using correlation and UPGMA) was performed. A custom C# program was run that sliced through the hierarchy at any number of levels (termed tiers). The program operates in one unit at a time—a 'node set.' Each node set would have some number of genes and the total number of genes would be represented by the total node sets across the tier. For each node set, the values for a particular morphological parameter from the member genes were averaged. The data were represented graphically as a cluster heat map, where each tier is a row in the graph, and a node set is a rectangle, colored by its average value. Statistics fit the cluster averages with a bootstrap sample from the entire data set. Significances are indicated by diamonds and asterisks. Diamonds indicate 'spiked bootstrap'—the family had a significant average when considering it against random picks always including the maximum or minimum value of the parameter (similar to first inverse jackknife) (Efron and Tibshirani, 1994). Asterisks indicate the family had a significant average, even after correcting for multiple comparisons per tier by Benjamini/Hochberg methods (Benjamini and Hochberg, 1995) (α=0.05). The analyses were run separately for each parameter tested, and significant values were summarized.

Pathway gene cluster analysis

Pathway information was garnered from Entrez Gene through linking to Reactome (http://www.reactome.org/) and KEGG, (http://www.genome.jp/kegg/pathway.html) (April 2009). Pathway annotations were found for 49% of the genes. KEGG not only provides pathway annotation, but also has a hierarchical representation of the pathways, so was chosen for further analyses. The hierarchical categories, subcategories, and pathways themselves were columns of a table, and genes were in each row. If a gene (e.g. IKBKB) was a member of the 'Pancreatic cancer' pathway, then it was assigned a 1 in that column, a 1 in the column '5.1 Cancers,' and a 1 in the column '5 human diseases.' In this cluster analysis, genes were allowed to be duplicated, so IKBKB had other rows in the table, and was assigned with the information for other pathways as well (chronic myeloid leukemia, prostate cancer, small cell lung cancer, type II diabetes mellitus, apoptosis, B-cell receptor signaling, T-cell receptor signaling, Toll-like receptor signaling, adipocytokine signaling, insulin signaling, MAPK signaling). Pathways with fewer than two genes were excluded. Average values were taken for each group, and displayed on a heat map as before. Here, a small square symbol indicates the family had a significant average but failed to be significant after corrections, and diamonds indicate significance compared with bootstrap replicates always including the maximum or minimum value of the parameter being tested (spiked bootstrap). When moving to lower tiers, genes were not allowed to be duplicated within a group, but were allowed to be duplicated between groups.

Supplementary information

Supplementary information is available at the *Molecular Systems Biology* website (http://www.nature.com/msb).

Acknowledgements

We are grateful to Murray Blackmore for assisting with many experiments and for thoughtful discussions. We thank the members of the LemBix laboratory for assistance with many phases of the project, especially Yan Shi, Daniel Gonzalez, Anthony Oliva, and Yuanyuan Jia. We thank Nirupa Chaudhari for providing the cDNA encoding the human PKA catalytic α subunit. This work was funded by the US Army (W81XWH-05-1-0061), the NIH (NICHD HD057632, NINDS NS059866), and The Miami Project to Cure Paralysis. WJB was a Lois Pope LIFE Fellow, with support from NINDS training grants T32 NS07492 and T32 NS007459. VPL holds the Walter G Ross Distinguished Chair in Developmental Neuroscience.

Conflict of interest

The authors declare that they have no conflict of interest.

References

Alessi DR, James SR, Downes CP, Holmes AB, Gaffney PR, Reese CB, Cohen P (1997) Characterization of a 3-phosphoinositide-dependent protein kinase which phosphorylates and activates protein kinase Balpha. *Curr Biol* **7:** 261–269

Anneren C, Reedquist KA, Bos JL, Welsh M (2000) GTK, a Src-related tyrosine kinase, induces nerve growth factor-independent neurite outgrowth in PC12 cells through activation of the Rap1 pathway. Relationship to Shb tyrosine phosphorylation and elevated levels of focal adhesion kinase. *J Biol Chem* **275:** 29153–29161

Arimura N, Kaibuchi K (2007) Neuronal polarity: from extracellular signals to intracellular mechanisms. *Nat Rev Neurosci* **8:** 194–205

Atwal JK, Massie B, Miller FD, Kaplan DR (2000) The TrkB-Shc site signals neuronal survival and local axon growth via MEK and P13-kinase. *Neuron* **27:** 265–277

Baronvanevercooren A, Kleinman HK, Ohno S, Marangos P, Schwartz JP, Duboisdalcq ME (1982) Nerve growth-factor, laminin, and fibronectin promote neurite growth in human-fetal sensory ganglia cultures. *J Neurosci Res* **8:** 179–193

Beggs HE, Soriano P, Maness PF (1994) NCAM-dependent neurite outgrowth is inhibited in neurons from Fyn-minus mice. *J Cell Biol* **127:** 825–833

Behrens A, Sibilia M, Wagner EF (1999) Amino-terminal phosphorylation of c-Jun regulates stress-induced apoptosis and cellular proliferation. *Nat Genet* **21:** 326–329

Benjamini Y, Hochberg Y (1995) Controlling the false discovery rate—a practical and powerful approach to multiple testing. *J Roy Stat Soc Series B-Methodol* **57:** 289–300

Bermingham-McDonogh O, McCabe KL, Reh TA (1996) Effects of GGF/neuregulins on neuronal survival and neurite outgrowth correlate with erbB2/neu expression in developing rat retina. *Development* **122:** 1427–1438

Bixby JL (1989) Protein kinase C is involved in laminin stimulation of neurite outgrowth. *Neuron* **3:** 287–297

Blackmore MG, Moore DL, Smith RP, Goldberg JL, Bixby JL, Lemmon VP (2010) High content screening of cortical neurons identifies novel regulators of axon growth. *Mol Cell Neurosci* **44:** 43–54

Bolis A, Coviello S, Bussini S, Dina G, Pardini C, Previtali SC, Malaguti M, Morana P, Del Carro U, Feltri ML, Quattrini A, Wrabetz L, Bolino A (2005) Loss of Mtmr2 phosphatase in Schwann cells but not in motor neurons causes Charcot-Marie-Tooth type 4B1 neuropathy with myelin outfoldings. *J Neurosci* **25:** 8567–8577

Borodinsky LN, O'Leary D, Neale JH, Vicini S, Coso OA, Fiszman ML (2003) GABA-induced neurite outgrowth of cerebellar granule cells is mediated by GABA(A) receptor activation, calcium influx and CaMKII and erk1/2 pathways. *J Neurochem* **84:** 1411–1420

Brede G, Solheim J, Stang E, Prydz H (2003) Mutants of the protein serine kinase PSKH1 disassemble the Golgi apparatus. *Exp Cell Res* **291:** 299–312

Brennan C, Monschau B, Lindberg R, Guthrie B, Drescher U, Bonhoeffer F, Holder N (1997) Two Eph receptor tyrosine kinase ligands control axon growth and may be involved in the creation of the retinotectal map in the zebrafish. *Development* **124:** 655–664

Caenepeel S, Charydczak G, Sudarsanam S, Hunter T, Manning G (2004) The mouse kinome: discovery and comparative genomics of all mouse protein kinases. *Proc Natl Acad Sci USA* **101:** 11707–11712

Chen B, Hammonds-Odie L, Perron J, Masters BA, Bixby JL (2002) SHP-2 mediates target-regulated axonal termination and NGF-dependent neurite growth in sympathetic neurons. *Dev Biol* **252:** 170–187

Chen YM, Wang QJ, Hu HS, Yu PC, Zhu J, Drewes G, Piwnica-Worms H, Luo ZG (2006) Microtubule affinity-regulating kinase 2 functions downstream of the PAR-3/PAR-6/atypical PKC complex in regulating hippocampal neuronal polarity. *Proc Natl Acad Sci USA* **103:** 8534–8539

Chijiwa T, Mishima A, Hagiwara M, Sano M, Hayashi K, Inoue T, Naito K, Toshioka T, Hidaka H (1990) Inhibition of forskolin-induced neurite outgrowth and protein phosphorylation by a newly synthesized selective inhibitor of cyclic AMP-dependent protein kinase, N-[2-(p-bromocinnamylamino)ethyl]-5-isoquinolinesulfonamide (H-89), of PC12D pheochromocytoma cells. *J Biol Chem* **265:** 5267–5272

Collinet C, Stoter M, Bradshaw CR, Samusik N, Rink JC, Kenski D, Habermann B, Buchholz F, Henschel R, Mueller MS, Nagel WE, Fava E, Kalaidzidis Y, Zerial M (2010) Systems survey of endocytosis by multiparametric image analysis. *Nature* **464:** 243–249

Coulonval K, Vandeput F, Stein RC, Kozma SC, Lamy F, Dumont JE (2000) Phosphatidylinositol 3-kinase, protein kinase B and ribosomal S6 kinases in the stimulation of thyroid epithelial cell proliferation by cAMP and growth factors in the presence of insulin. *Biochem J* **348**(Part 2)**:** 351–358

Da Silva JS, Hasegawa T, Miyagi T, Dotti CG, Abad-Rodriguez J (2005) Asymmetric membrane ganglioside sialidase activity specifies axonal fate. *Nat Neurosci* **8:** 606–615

Daniels RH, Hall PS, Bokoch GM (1998) Membrane targeting of p21-activated kinase 1 (PAK1) induces neurite outgrowth from PC12 cells. *EMBO J* **17:** 754–764

Davare MA, Fortin DA, Saneyoshi T, Nygaard S, Kaech S, Banker G, Soderling TR, Wayman GA (2009) Transient receptor potential canonical 5 channels activate Ca2 + /calmodulin kinase Igamma to promote axon formation in hippocampal neurons. *J Neurosci* **29:** 9794–9808

Desai CJ, Krueger NX, Saito H, Zinn K (1997) Competition and cooperation among receptor tyrosine phosphatases control motoneuron growth cone guidance in Drosophila. *Development* **124:** 1941–1952

Dey N, Howell BW, De PK, Durden DL (2005) CSK negatively regulates nerve growth factor induced neural differentiation and augments AKT kinase activity. *Exp Cell Res* **307:** 1–14

Dill J, Wang H, Zhou F, Li S (2008) Inactivation of glycogen synthase kinase 3 promotes axonal growth and recovery in the CNS. *J Neurosci* **28:** 8914–8928

Dotti CG, Sullivan CA, Banker GA (1988) The establishment of polarity by hippocampal neurons in culture. *J Neurosci* **8:** 1454–1468

Efron B, Tibshirani RJ (1993) An introduction to the bootstrap. In *Monographs on Statistics and Applied Probability Series*, Vol. 57, New Edition, pp 1–436. New York: Chapman & Hall/CRC

Enomoto H, Crawford PA, Gorodinsky A, Heuckeroth RO, Johnson EM, Milbrandt J (2001) RET signaling is essential for migration, axonal growth and axon guidance of developing sympathetic neurons. *Development* **128:** 3963–3974

Esch T, Lemmon V, Banker G (1999) Local presentation of substrate molecules directs axon specification by cultured hippocampal neurons. *J Neurosci* **19:** 6417–6426

Figueroa JD, Benton RL, Velazquez I, Torrado AI, Ortiz CM, Hernandez CM, Diaz JJ, Magnuson DS, Whittemore SR, Miranda JD (2006) Inhibition of EphA7 up-regulation after spinal cord injury reduces apoptosis and promotes locomotor recovery. *J Neurosci Res* **84:** 1438–1451

Firestein R, Cleary ML (2001) Pseudo-phosphatase Sbf1 contains an N-terminal GEF homology domain that modulates its growth regulatory properties. *J Cell Sci* **114:** 2921–2927

Gerhard DS, Wagner L, Feingold EA, Shenmen CM, Grouse LH, Schuler G, Klein SL, Old S, Rasooly R, Good P, Guyer M, Peck AM, Derge JG, Lipman D, Collins FS, Jang W, Sherry S, Feolo M, Misquitta L, Lee E, *et al.*, MGC Project Team (2004) The status, quality, and expansion of the NIH full-length cDNA project: the Mammalian Gene Collection (MGC). *Genome Res* **14:** 2121–2127

Goldshmit Y, Galea MP, Wise G, Bartlett PF, Turnley AM (2004) Axonal regeneration and lack of astrocytic gliosis in EphA4-deficient mice. *J Neurosci* **24:** 10064–10073

Goslin K, Asmussen H, Banker GA (1998) Rat hippocampal neurons in low-density cultures. In *Culturing Nerve Cells* (Banker GA, Goslin K, eds). Cambridge, MA: MIT Press

Gu C, Shim S, Shin J, Kim J, Park J, Han K, Park S (2005) The EphA8 receptor induces sustained MAP kinase activation to promote neurite outgrowth in neuronal cells. *Oncogene* **24:** 4243–4256

Haines BP, Gupta R, Jones CM, Summerbell D, Rigby PW (2005) The NLRR gene family and mouse development: modified differential display PCR identifies NLRR-1 as a gene expressed in early somitic myoblasts. *Dev Biol* **281:** 145–159

Hatada S, Kinoshita M, Takahashi S, Nishihara R, Sakumoto H, Fukui A, Noda M, Asashima M (1997) An interferon regulatory factor-

related gene (xIRF-6) is expressed in the posterior mesoderm during the early development of Xenopus laevis. *Gene* **203:** 183–188

Hausott B, Schlick B, Vallant N, Dorn R, Klimaschewski L (2008) Promotion of neurite outgrowth by fibroblast growth factor receptor 1 overexpression and lysosomal inhibition of receptor degradation in pheochromocytoma cells and adult sensory neurons. *Neuroscience* **153:** 461–473

Heber S, Herms J, Gajic V, Hainfellner J, Aguzzi A, Rulicke T, Kretzschmar H, von Koch C, Sisodia S, Tremml P, Lipp HP, Wolfer DP, Muller U (2000) Mice with combined gene knock-outs reveal essential and partially redundant functions of amyloid precursor protein family members. *J Neurosci* **20:** 7951–7963

Hemmati-Brivanlou A, Melton DA (1992) A truncated activin receptor inhibits mesoderm induction and formation of axial structures in Xenopus embryos. *Nature* **359:** 609–614

Huang EJ, Reichardt LF (2003) Trk receptors: roles in neuronal signal transduction. *Annu Rev Biochem* **72:** 609–642

Huang Z, Zang K, Reichardt LF (2005) The origin recognition core complex regulates dendrite and spine development in postmitotic neurons. *J Cell Biol* **170:** 527–535

Ignelzi Jr MA, Miller DR, Soriano P, Maness PF (1994) Impaired neurite outgrowth of src-minus cerebellar neurons on the cell adhesion molecule L1. *Neuron* **12:** 873–884

Ishii T, Satoh E, Nishimura M (2001) Integrin-linked kinase controls neurite outgrowth in N1E-115 neuroblastoma cells. *J Biol Chem* **276:** 42994–43003

Ivankovic-Dikic I, Gronroos E, Blaukat A, Barth BU, Dikic I (2000) Pyk2 and FAK regulate neurite outgrowth induced by growth factors and integrins. *Nat Cell Biol* **2:** 574–581

Kanehisa M, Goto S, Kawashima S, Okuno Y, Hattori M (2004) The KEGG resource for deciphering the genome. *Nucleic Acids Res* **32:** D277–D280

Kao HT, Song HJ, Porton B, Ming GL, Hoh J, Abraham M, Czernik AJ, Pieribone VA, Poo MM, Greengard P (2002) A protein kinase A-dependent molecular switch in synapsins regulates neurite outgrowth. *Nat Neurosci* **5:** 431–437

Kishi M, Pan YA, Crump JG, Sanes JR (2005) Mammalian SAD kinases are required for neuronal polarization. *Science* **307:** 929–932

Klein R (2001) Excitatory Eph receptors and adhesive ephrin ligands. *Curr Opin Cell Biol* **13:** 196–203

Kolkova K, Novitskaya V, Pedersen N, Berezin V, Bock E (2000) Neural cell adhesion molecule-stimulated neurite outgrowth depends on activation of protein kinase C and the Ras-mitogen-activated protein kinase pathway. *J Neurosci* **20:** 2238–2246

Koprivica V, Cho KS, Park JB, Yiu G, Atwal J, Gore B, Kim JA, Lin E, Tessier-Lavigne M, Chen DF, He Z (2005) EGFR activation mediates inhibition of axon regeneration by myelin and chondroitin sulfate proteoglycans. *Science* **310:** 106–110

Kuo WL, Chung KC, Rosner MR (1997) Differentiation of central nervous system neuronal cells by fibroblast-derived growth factor requires at least two signaling pathways: roles for Ras and Src. *Mol Cell Biol* **17:** 4633–4643

Larkin MA, Blackshields G, Brown NP, Chenna R, McGettigan PA, McWilliam H, Valentin F, Wallace IM, Wilm A, Lopez R, Thompson JD, Gibson TJ, Higgins DG (2007) Clustal W and Clustal X version 2.0. *Bioinformatics* **23:** 2947–2948

Lautermilch NJ, Spitzer NC (2000) Regulation of calcineurin by growth cone calcium waves controls neurite extension. *J Neurosci* **20:** 315–325

Lazarovici P, Dickens G, Kuzuya H, Guroff G (1987) Long-term, heterologous down-regulation of the epidermal growth factor receptor in PC12 cells by nerve growth factor. *J Cell Biol* **104:** 1611–1621

Lee HC, Tsai JN, Liao PY, Tsai WY, Lin KY, Chuang CC, Sun CK, Chang WC, Tsai HJ (2007) Glycogen synthase kinase 3 alpha and 3 beta have distinct functions during cardiogenesis of zebrafish embryo. *BMC Dev Biol* **7:** 93

Lin D, Edwards AS, Fawcett JP, Mbamalu G, Scott JD, Pawson T (2000) A mammalian PAR-3-PAR-6 complex implicated in Cdc42/Rac1 and aPKC signalling and cell polarity. *Nat Cell Biol* **2:** 540–547

Lin HY, Xu J, Ornitz DM, Halegoua S, Hayman MJ (1996) The fibroblast growth factor receptor-1 is necessary for the induction of neurite outgrowth in PC12 cells by aFGF. *J Neurosci* **16:** 4579–4587

Loh SHY, Francescut L, Lingor P, Bahr M, Nicotera P (2008) Identification of new kinase clusters required for neurite outgrowth and retraction by a loss-of-function RNA interference screen. *Cell Death Differ* **15:** 283–298

Maness PF, Schachner M (2007) Neural recognition molecules of the immunoglobulin superfamily: signaling transducers of axon guidance and neuronal migration. *Nat Neurosci* **10:** 19–26

Manning G, Whyte DB, Martinez R, Hunter T, Sudarsanam S (2002) The protein kinase complement of the human genome. *Science* **298:** 1912–1934

Marcus M, Nielsen K, Goitein R, Gropp A (1979) Pattern of condensation of mouse and Chinese hamster chromosomes in G2 and mitosis of 33258-Hoechst-treated cells. *Exp Cell Res* **122:** 191–201

Markus A, Zhong J, Snider WD (2002) Raf and akt mediate distinct aspects of sensory axon growth. *Neuron* **35:** 65–76

Menager C, Arimura N, Fukata Y, Kaibuchi K (2004) PIP3 is involved in neuronal polarization and axon formation. *J Neurochem* **89:** 109–118

Mendes SW, Henkemeyer M, Liebl DJ (2006) Multiple Eph receptors and B-class ephrins regulate midline crossing of corpus callosum fibers in the developing mouse forebrain. *J Neurosci* **26:** 882–892

Meyer-Franke A, Kaplan MR, Pfrieger FW, Barres BA (1995) Characterization of the signaling interactions that promote the survival and growth of developing retinal ganglion cells in culture. *Neuron* **15:** 805–819

Moore DL, Blackmore MG, Hu Y, Kaestner KH, Bixby JL, Lemmon VP, Goldberg JL (2009) KLF family members regulate intrinsic axon regeneration ability. *Science* **326:** 298–301

Morita N, Takumi T, Kiyama H (1996) Distinct localization of two serine-threonine kinase receptors for activin and TGF-beta in the rat brain and down-regulation of type I activin receptor during peripheral nerve regeneration. *Brain Res Mol Brain Res* **42:** 263–271

Morooka T, Nishida E (1998) Requirement of p38 mitogen-activated protein kinase for neuronal differentiation in PC12 cells. *J Biol Chem* **273:** 24285–24288

Myers RR, Sekiguchi Y, Kikuchi S, Scott B, Medicherla S, Protter A, Campana WM (2003) Inhibition of p38 MAP kinase activity enhances axonal regeneration. *Exp Neurol* **184:** 606–614

Nakagawara A (2001) Trk receptor tyrosine kinases: a bridge between cancer and neural development. *Cancer Lett* **169:** 107–114

Namikawa K, Honma M, Abe K, Takeda M, Mansur K, Obata T, Miwa A, Okado H, Kiyama H (2000) Akt/protein kinase B prevents injury-induced motoneuron death and accelerates axonal regeneration. *J Neurosci* **20:** 2875–2886

Nara K, Akasako Y, Matsuda Y, Fukazawa Y, Iwashita S, Kataoka M, Nagai Y (2001) Cloning and characterization of a novel serine/threonine protein kinase gene expressed predominantly in developing brain. *Eur J Biochem* **268:** 2642–2651

Nikolic M, Chou MM, Lu W, Mayer BJ, Tsai LH (1998) The p35/Cdk5 kinase is a neuron-specific Rac effector that inhibits Pak1 activity. *Nature* **395:** 194–198

Nimmo GA, Cohen P (1978) Regulation of glycogen-metabolism—purification and characterization of protein phosphatase inhibitor-1 from rabbit skeletal-muscle. *Eur J Biochem* **87:** 341–351

Oliva Jr AA, Atkins CM, Copenagle L, Banker GA (2006) Activated c-Jun N-terminal kinase is required for axon formation. *J Neurosci* **26:** 9462–9470

Park KK, Liu K, Hu Y, Smith PD, Wang C, Cai B, Xu B, Connolly L, Kramvis I, Sahin M, He Z (2008) Promoting axon regeneration in the adult CNS by modulation of the PTEN/mTOR pathway. *Science* **322:** 963–966

Robinson MJ, Stippec SA, Goldsmith E, White MA, Cobb MH (1998) A constitutively active and nuclear form of the MAP kinase ERK2 is sufficient for neurite outgrowth and cell transformation. *Curr Biol* **8:** 1141–1150

Sacher R, Stergiou L, Pelkmans L (2008) Lessons from genetics: interpreting complex phenotypes in RNAi screens. *Curr Opin Cell Biol* **20:** 483–489

Sasaguri H, Mitani T, Anzai M, Kubodera T, Saito Y, Yamada H, Mizusawa H, Yokota T (2009) Silencing efficiency differs among tissues and endogenous microRNA pathway is preserved in short hairpin RNA transgenic mice. *FEBS Lett* **583:** 213–218

Schmidt A, Durgan J, Magalhaes A, Hall A (2007) Rho GTPases regulate PRK2/PKN2 to control entry into mitosis and exit from cytokinesis. *EMBO J* **26:** 1624–1636

Sepp KJ, Hong P, Lizarraga SB, Liu JS, Mejia LA, Walsh CA, Perrimon N (2008) Identification of neural outgrowth genes using genome-wide RNAi. *PLoS Genet* **4:** e1000111

Shaner NC, Campbell RE, Steinbach PA, Giepmans BN, Palmer AE, Tsien RY (2004) Improved monomeric red, orange and yellow fluorescent proteins derived from Discosoma sp. red fluorescent protein. *Nat Biotechnol* **22:** 1567–1572

Shelly M, Lim BK, Cancedda L, Heilshorn SC, Gao H, Poo MM (2010) Local and long-range reciprocal regulation of cAMP and cGMP in axon/dendrite formation. *Science* **327:** 547–552

Shibata A, Laurent CE, Smithgall TE (2003) The c-Fes protein-tyrosine kinase accelerates NGF-induced differentiation of PC12 cells through a PI3K-dependent mechanism. *Cell Signal* **15:** 279–288

Shu X, Shaner NC, Yarbrough CA, Tsien RY, Remington SJ (2006) Novel chromophores and buried charges control color in mFruits. *Biochemistry* **45:** 9639–9647

Simpson KJ, Selfors LM, Bui J, Reynolds A, Leake D, Khvorova A, Brugge JS (2008) Identification of genes that regulate epithelial cell migration using an siRNA screening approach. *Nat Cell Biol* **10:** 1027–1038

Sosa L, Dupraz S, Laurino L, Bollati F, Bisbal M, Caceres A, Pfenninger KH, Quiroga S (2006) IGF-1 receptor is essential for the establishment of hippocampal neuronal polarity. *Nat Neurosci* **9:** 993–995

Spanner S, Ansell GB (1979) Choline kinase and ethanolamine kinase activity in the cytosol of nerve endings from rat forebrain. *Biochem J* **178:** 753–760

Stepanek L, Stoker AW, Stoeckli E, Bixby JL (2005) Receptor tyrosine phosphatases guide vertebrate motor axons during development. *J Neurosci* **25:** 3813–3823

Tang TS, Tu H, Wang Z, Bezprozvanny I (2003) Modulation of type 1 inositol (1,4,5)-trisphosphate receptor function by protein kinase a and protein phosphatase 1alpha. *J Neurosci* **23:** 403–415

Thompson JD, Higgins DG, Gibson TJ (1994) CLUSTAL W: improving the sensitivity of progressive multiple sequence alignment through sequence weighting, position-specific gap penalties and weight matrix choice. *Nucleic Acids Res* **22:** 4673–4680

Urrutia R, Henley JR, Cook T, McNiven MA (1997) The dynamins: redundant or distinct functions for an expanding family of related GTPases? *Proc Natl Acad Sci USA* **94:** 377–384

Vandenheuvel S, Harlow E (1993) Distinct roles for cyclin-dependent kinases in cell-cycle control. *Science* **262:** 2050–2054

Wayman GA, Kaech S, Grant WF, Davare M, Impey S, Tokumitsu H, Nozaki N, Banker G, Soderling TR (2004) Regulation of axonal extension and growth cone motility by calmodulin-dependent protein kinase I. *J Neurosci* **24:** 3786–3794

Wiggin GR, Soloaga A, Foster JM, Murray-Tait V, Cohen P, Arthur JS (2002) MSK1 and MSK2 are required for the mitogen- and stress-induced phosphorylation of CREB and ATF1 in fibroblasts. *Mol Cell Biol* **22:** 2871–2881

Wong EV, Schaefer AW, Landreth G, Lemmon V (1996) Involvement of p90(rsk) in neurite outgrowth mediated by the cell adhesion molecule L1. *J Biol Chem* **271:** 18217–18223

Wu G, Aoyama C, Young SG, Vance DE (2008) Early embryonic lethality caused by disruption of the gene for choline kinase alpha, the first enzyme in phosphatidylcholine biosynthesis. *J Biol Chem* **283:** 1456–1462

Wu GY, Cline HT (1998) Stabilization of dendritic arbor structure *in vivo* by CaMKII. *Science* **279:** 222–226

Xia ZG, Dickens M, Raingeaud J, Davis RJ, Greenberg ME (1995) Opposing effects of Erk and Jnk-P38 map kinases on apoptosis. *Science* **270:** 1326–1331

Xian CJ, Zhou XF (2004) EGF family of growth factors: essential roles and functional redundancy in the nerve system. *Front Biosci* **9:** 85–92

Yoshimura T, Kawano Y, Arimura N, Kawabata S, Kikuchi A, Kaibuchi K (2005) GSK-3beta regulates phosphorylation of CRMP-2 and neuronal polarity. *Cell* **120:** 137–149

